Effects on Aortoiliac Fluid Dynamics After Endovascular Sealing of Abdominal Aneurysms

Mariano E. Casciaro, PhD[1], Javier Dottori, PhD[2],
Salma El-Batti, MD[3], Jean-Marc Alsac, MD[3], Elie Mousseaux, MD[3],
Ignacio Larrabide, PhD[2], and Damian Craiem, PhD[1,3]

Abstract

Objectives: To evaluate the effects on aortoiliac fluid dynamics after the implantation of an endograft based on endovascular aneurysm sealing (EVAS) versus endovascular aneurysm repair (EVAR) strategy. **Methods:** An adaptive geometrical deformable model was used for aortic lumen segmentation in 8 patients before and after the surgery. Abdominal aneurysms were treated with an endograft based on the EVAS system (Nellix, n = 4) and with a device based on an anatomical fixation technology (n = 4). Pressure, blood velocity, and wall shear stress (WSS) were estimated at different aortic regions using computational fluid dynamics methods. Physiologic inlet/outlet flow values at the abdominal aorta, the celiac trunk, and the mesenteric and the renal arteries were set. Pressure references were set at iliac arteries outlet. **Results:** Maximum aneurysm sizes were similar for both groups in the preoperative scans. The lumen area was lower after EVAR ($P < .05$) and EVAS ($P < .01$) compared to preoperative aortic lumen sizes. Pressure increase was higher in the proximal abdominal aorta after EVAS compared to EVAR (2.3 ± 0.3 mm Hg vs 0.9 ± 0.3 mm Hg, $P < .001$). Peak blood velocities inside the endografts were 3-fold higher for EVAS compared to EVAR (54 ± 5 cm/s vs 17 ± 4 cm/s, $P < .01$). Velocities at the iliac arteries also remained higher for EVAS (38 ± 4 cm/s vs 24 ± 4 cm/s, $P < .05$). Peak WSS at the iliac arteries remained higher for EVAS compared to EVAR group ($P < .05$). **Conclusion:** The significant modification of the aortic bifurcation anatomy after EVAS alters aortoiliac fluid dynamics, showing a pressure impact at the renal arteries level and an acceleration of the blood velocity at the iliac region with a concomitant increase in peak WSS.

Keywords

abdominal aortic aneurysm, Nellix endograft, computational fluid dynamics, geometric deformable models, sac anchoring prosthesis, endovascular repair

Introduction

The Nellix endograft (Endologix, Irvine, California) proposes to treat infrarenal abdominal aortic aneurysms (AAAs) based on the endovascular aneurysm sealing (EVAS) system.[1] Unlike in conventional endovascular aneurysm repair (EVAR), where most endografts include a proximal fixation mechanism, the EVAS system is composed of 2 stents surrounded by expandable endobags that are filled with a polymer to seal the aneurysm sac (Figure 1). As EVAS technology aimed for a continuous sealing all along the internal surface of the aneurysm lumen, expectations about endoleak and graft migration prevention have been raised.[2] However, the configuration of the abdominal aorta anatomy, from the renal arteries to the aortic bifurcation, is considerably altered using this technique. To seal the aneurysm, the blood is forced to rapidly flow into two 10-mm stents just below the renal arteries. In particular, we hypothesize that this upward relocation of the aortic bifurcation might induce a modification in flow patterns in the renal and iliac regions.

So far, limited data are available regarding volumetric anatomic modifications of the AAA after graft implantation. Some reports on post-EVAS changes have shown small but significant increases in aortic lumen and aneurysm volumes compared to preoperative scans.[3,4] Other groups have found that aneurysm volume, neck diameter, and renal angulations remained unchanged after implantation and observed a slight straightening of the iliac arteries.[5] The characterization of fluid dynamics in 3 different endograft models (including the EVAS system) was recently reported using laser particle imaging velocimetry (PIV) measured on phantoms.[6] However, the
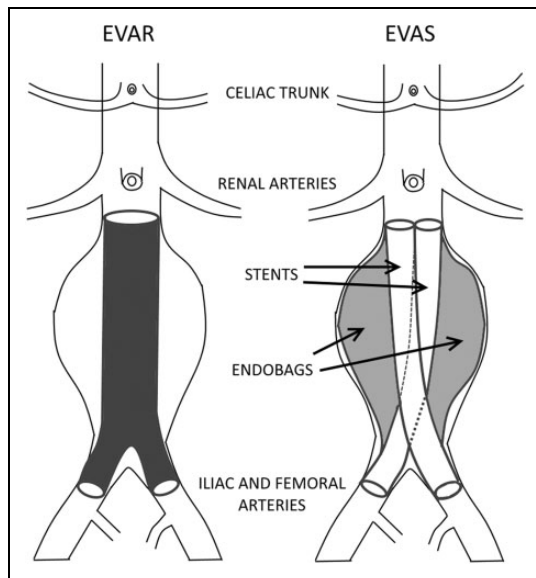
[1]Instituto de Medicina Traslacional, Trasplante y Bioingeniería (IMeTTyB), Universidad Favaloro-CONICET, Buenos Aires, Argentina
[2]PLADEMA, CONICET, UNICEN, Tandil, Argentina
[3]APHP, Hôpital Européen Georges Pompidou, Paris, France

Corresponding Author:
Damian Craiem, Solis 453 (CP 1078), Buenos Aires, Argentina.
Email: dcraiem@favaloro.edu.ar

Figure 1. Schematic representation of an endovascular aneurysm repair (EVAR) using an anatomical fixation technology (AFX) device and an endovascular aneurysm sealing (EVAS) with the Nellix endograft.

impact of the anatomical modifications on flow dynamics in terms of pressure, velocity, and wall shear stress (WSS) has not been studied until now using true 3-D meshes obtained from real cases.

The objectives of this study were to quantify and compare the hemodynamic changes following EVAS versus EVAR. The causes of blood flow differences in terms of pressure, blood velocity, and WSS were analyzed and discussed to identify possible clinical implications. Patient-specific meshes were reconstructed using enhanced computed tomography images from pre- and postoperative studies. Estimations of pressure, blood velocity, and WSS, at different regions of the abdominal aorta, were simulated to assess differences following EVAS versus EVAR using validated computational fluid dynamics (CFD) methods.[7,8]

Methods

Study Sample

Data from patients who underwent an infrarenal aortic aneurysm endovascular repair between January and June 2014 in the Hôpital Européen Georges Pompidou (Paris, France) were retrospectively reviewed. Patients who were treated with Nellix or anatomical fixation technology (AFX) devices within the study period were selected and those with comparable external aortic diameter were included. We excluded patients who were treated with other devices than Nellix or AFX. Eight patients (all men, age range: 69-87 years) with noncomplicated AAA were finally included in this study. Each patient signed an approved informed consent before the surgery. The retrospective analysis of personal health data of study patients had the authorization of the Commission Nationale de l'Informatique

et des Libertés and was in accordance with the Declaration of Helsinki. This project was part of an internal evaluation of the EVAS system at our institution, and thus, formal approval from the institutional review board was not required. Patients were treated using either the EVAS technology (Nellix) or an endograft based on an AFX. Pre- and postoperative contrast-enhanced computed tomography scans were used to build finite element meshes using an automated method to isolate the abdominal aorta lumen. Afterward, the meshes were employed in the CFD simulations to quantify aortoiliac fluid dynamics.

Endovascular Procedure

The implantation procedure for the Nellix system has been previously described.[1] Patients who received the Nellix device were selected based on their preoperative anatomy, including short infrarenal neck and high risk of postoperative type II endoleaks. The EVAR procedure included the implantation of an AFX endograft. This endograft has a more physiologic configuration with a long main body and 2 innate limbs. It is deployed so that it rests on the native aortoiliac bifurcation, using an anatomical fixation for stabilization. Additionally, this endograft might be more conformable to blood flow compared to other technologies as the e-PTFE is external to the stent struts. Details of the endograft and the procedure can be found elsewhere.[9]

Abdominal Aorta Segmentation

A geometric deformable model (GDM), originally proposed to quantify aneurysm lumen volume,[4] was used for the abdominal aorta segmentation before and after endograft implantation. Briefly, the GDM segmentation emulates a virtual elastic balloon that inflates inside a region of interest. The GDM initial shape is a sphere composed by nodes and triangular faces with its vertices connected by elastic edges. A controlled force simulates the inflation of the sphere. Different internal forces (stretching, bending, and dissipative forces) are calculated for each vertex in parallel, taking into account the intensities in Hounsfield units of the surrounding structures. The size of the triangular faces remain stable, controlled by a collapse/subdivide algorithm. The adaptation process continues until the deformable mesh fits the lumen shape and until equilibrium is obtained. In pre- and postoperative scans, a single deformable balloon was positioned inside the proximal abdominal aorta lumen at the level of the renal artery. The GDM was allowed to grow upward until the diaphragm level and downward to fill the aortic lumen and the left and right common iliac arteries. The reader can find a more complete mathematical and algorithmic explanation elsewhere.[4]

Aortic Mesh Generation

The aortic lumen meshes were postprocessed to obtain watertight surfaces, proper for CFD simulations. AngioLab (version 0.9) software was used for the mesh edition, smoothing, mesh improvement, and preprocessing.[8] Small vessels were

eliminated. Superior mesenteric, celiac trunk, left and right renal arteries, left and right iliac arteries, and left and right femoral arteries were perpendicularly cut. The cut was placed between 5 and 10 diameters away from the branching point. All proximal and distal endpoints were cut at the same location for matching pre- and posttreatment models. The boundaries were extruded with a regular cylinder to facilitate the development of flow boundary conditions.

Numerical Simulations

Validated CFD simulations were performed to estimate pressure, flow velocity, and WSS[7,8] at 6 different regions (R1-R6) orthogonal to aortic centerline:

- Inlet region (R1): 1 cm above celiac trunk (inlet region),
- Celiac region (R2): near the celiac trunk,
- Mesenteric region (R3): near the mesenteric artery,
- Renal region (R4): between the 2 renal arteries,
- Aneurysm region (R5): at the level of the maximum diameter evaluated in the preoperative scan, and
- Common iliac artery region (R6): before the internal iliac artery bifurcation.

Fluid flow has been largely studied in physics, mathematics, and mechanics using mathematical models that describe the movement of a fluid in a confined reservoir, like the flow of blood inside vessels. Such mathematical models are the so-called Navier-Stokes equations. In most real situations, it is not possible to find the exact mathematical expression to solve them and numerical solutions are approximated by using a proper discretization of space and time. The CFD is the set of techniques and algorithms that allow finding such numerical approximations at the cost of computationally intensive calculations. Different commercial and free software packages for CFD are currently available. Open source Finite Volume software OpenFOAM (OpenFOAM, Bracknell, United Kingdom) was used for CFD analysis in our study.[10] A stationary solver (simpleFoam [version 4.1]), available in the software, was used to compute the numerical solution of Navier-Stokes equations.[11] Blood was considered a Newtonian fluid and dynamic viscosities constant ($\mu = 0.004$ Pa·s).[12] Other simplifications for the simulation included a continuous rather than pulsatile flow condition, a rigid aortic wall, and the absence of mural thrombus assumption. Generated meshes contained between 140 000 and 200 000 elements.[13]

Inlet flow for CFD simulations was set to 3.5 L/min, and outlet boundary conditions at the renal arteries, the superior mesenteric artery, and the celiac trunk were set to -0.5 L/min to reproduce normal physiological values based on the literature.[14-16] Pressure zero references were set at each external and internal iliac outlet. These conditions were maintained across all simulations.

Measurements and Statistical Analysis

A single expert (J.-M.A.) measured the preoperative anatomy of every aneurysm, including the diameters of the aortic neck,

Table 1. Initial Aortic Aneurysm Anatomy.

Attribute	EVAS Group	EVAR Group
Aortic neck diameter, mm	23.0 ± 2.4	20.8 ± 2.2
Aortic neck length, mm	12.5 ± 2.1	32.5 ± 9.0[a]
Aortic neck angle, °	37.8 ± 13.4	19.8 ± 16.2
Aortic aneurysm external diameter, mm	59.0 ± 4.7	58.5 ± 6.7
Aortic aneurysm lumen diameter, mm	40.3 ± 4.6	43.3 ± 9
Left iliac artery diameter, mm	14.8 ± 1.3	13.8 ± 2.9
Right iliac artery diameter, mm	14.0 ± 1.4	13.5 ± 2.6
Left iliac stent covered length, mm	34.0 ± 10.2	37.3 ± 9.3
Right iliac stent covered length, mm	34.3 ± 10.7	35.0 ± 9.7

Abbreviations: EVAR, endovascular aneurysm repair; EVAS, endovascular aneurysm sealing.
[a]$P < .01$.

the aneurysm, and the iliac arteries. The aortic neck length and angulation were also manually estimated. For every mesh and at each region, the following calculations were done: (1) cross-sectional area (CSA), (2) relative pressure compared to the outlet flow at the external iliac artery, (3) 95th percentile of blood flow velocities, and (4) 95th percentile of WSS. Patients were separated into the EVAS and EVAR group. For the estimation of the CSA at the iliac region, the sum of the 2 iliac arteries areas was calculated. Similarly, the CSA for the aneurysm region was calculated from areas of the 2 stents inside the Nellix endoframe. Left and right limbs pressure, velocity, and WSS values were averaged. Mean and standard deviations were used to summarize the aortic measurements in each group. A paired Wilcoxon test was used to compare pre- and postoperative values. Comparisons between groups were calculated with an unpaired Wilcoxon test. P values below 5% were considered significant.

Results

The preoperative anatomy of each aneurysm was manually assessed and geometric values were similar between groups, except for the aortic neck length that was shorter in the EVAS group ($P < .01$; Table 1). In the EVAR group, the mean size of the AFX endograft limbs was 18.0 ± 2.3 mm (16 mm for 2 patients and 20 mm for the other 2).

The aortic lumen meshes, before and after the procedure for each patient, are shown in Supplemental Figure 1. After EVAS, an upward relocation of the aortic bifurcation is clearly visible. Conversely, since the AFX endograft rests on the native aortic bifurcation, the aortoiliac anatomy was globally preserved after EVAR.

Lumen CSA of each region of the abdominal aorta is shown in Figure 2 for both groups before (PRE, solid lines) and after (POST, dotted and dashed lines) endograft implantation. Thicker traces were used for the curves of the EVAS group. In the preoperative scans, aneurysm size was similar between groups. In the postoperative scans, aortic size was significantly lower at the aneurysm region for the EVAR ($P < .05$) and the EVAS ($P < .01$) groups compared to preoperative values. Note
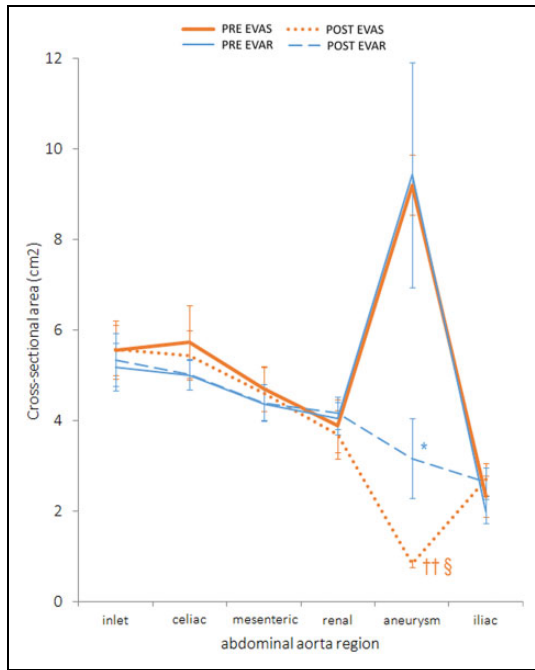
Figure 2. Mean cross-sectional areas for the different abdominal aorta regions before (PRE) and after (POST) implantation of the endografts. Dotted and dashed lines indicate post-endovascular aneurysm sealing (EVAS) and post-endovascular aneurysm (EVAR) cases, respectively. *$P < .05$ post-EVAR compared to pre-EVAR. $^{††}P < .01$ post-EVAS compared to pre-EVAS. $^{§}P < .05$ post-EVAS with respect to post-EVAR.
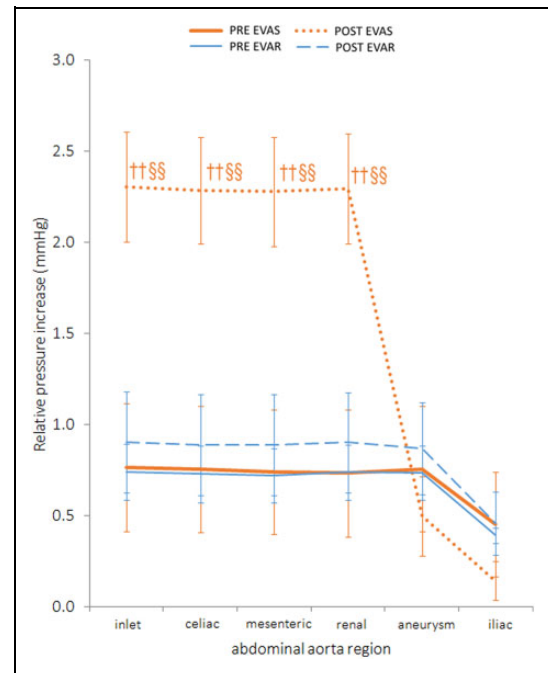
Table 2. Absolute Changes in Pressure, Velocity, and Wall Shear Stress Between Postoperative Minus Preoperative Scans Using Baseline Boundary Conditions From Table 1.

	EVAS Group	EVAR Group
Relative pressure, mm Hg		
Renal region	1.6 ± 0.9	0.2 ± 0.4[a]
Aneurysm region	-0.3 ± 0.4	0.1 ± 0.4
Iliac region	-0.3 ± 0.4	0.0 ± 0.2
Percentile 95th peak velocity, cm/s		
Renal region	-1.6 ± 2.2	-1.1 ± 1.1
Aneurysm region	42.1 ± 12.8	3.7 ± 4.4[a]
Iliac region	12.5 ± 18.3	-1.2 ± 5.7[b]
Percentile 95th WSS, Pa		
Renal region	-0.4 ± 0.8	0.1 ± 0.3
Aneurysm region	1.0 ± 0.2	0.4 ± 0.4[b]
Iliac region	0.6 ± 1.0	0.0 ± 0.4[b]

Abbreviations: EVAR, endovascular aneurysm repair; EVAS, endovascular aneurysm sealing.
[a]$P < .01$.
[b]$P < .05$.

that at this region, the blood circulates inside the 2 stents for the EVAS system endograft, forcing a narrower CSA compared to EVAR device ($P < .05$).

Postoperative minus preoperative absolute changes in pressure, velocity, and WSS between and scans are show in Table 2. Pressure values for the aortic regions (relative to the iliac outlet reference) are shown in Figure 3. In the preoperative scan, stable pressure values <1 mm Hg were observed in both groups above the aortic bifurcation and a linear reduction was observed toward the external iliac arteries. Pressure did not change after EVAR. However, a significant pressure rise was observed after EVAS above the endograft compared to both preoperative scan ($P < .01$) and EVAR group ($P < .01$). Post-EVAS, pressure values raised 1.6 ± 0.9 mm Hg compared to pre-EVAS (Table 2).

Peak blood velocities at different aortic regions are shown in Figure 4. During the preoperative scans of both groups, peak velocities decrease inside the aneurysm sac and accelerated entering the iliac arteries. After EVAS, blood significantly accelerated inside the stents compared to both preoperative scan ($P < .01$) and the EVAR group ($P < .01$). Mean absolute velocity changes were 42.1 ± 12.8 cm/s and 3.7 ± 4.4 cm/s for EVAS and EVAR groups, respectively. Blood velocity remained accelerated post-EVAS compared to the EVAR group at the iliac region ($P < .05$). Peak WSS values resulted more variable than velocities, but they globally followed the velocity behavior (Figure 5). Again, peak values inside the
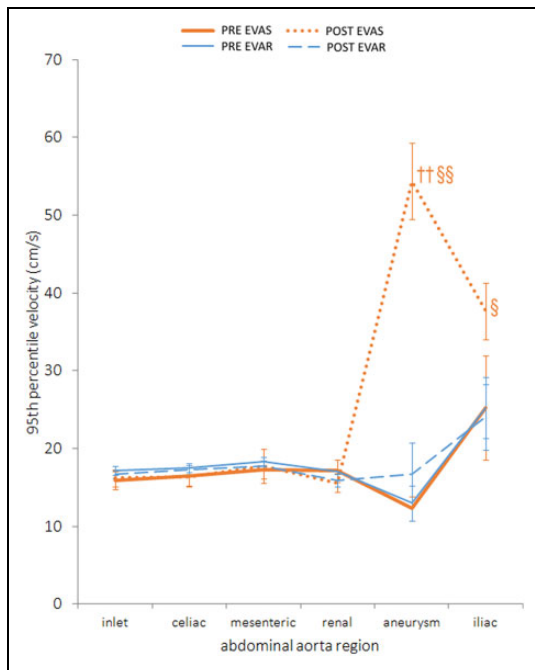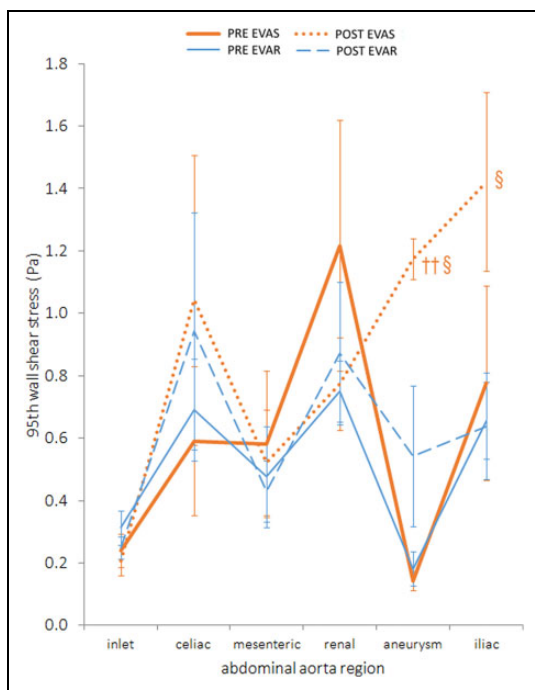

Figure 3. Mean relative pressure increase (with respect to iliac outlet pressure) for the different abdominal aorta regions before (PRE) and after (POST) implantation of the endografts. Dotted and dashed lines indicate post-endovascular aneurysm sealing (EVAS) and post-endovascular aneurysm repair (EVAR) cases, respectively. $^{††}P < .01$ post-EVAS compared to pre-EVAS. $^{§§}P < .01$ EVAS compared to EVAR.

stents were higher after EVAS compared to preoperative scans ($P < .01$) and the EVAR group ($P < .01$). Peak WSS values after EVAS remained higher at the iliac level compared to the EVAR group ($P < .05$). Finally, WSS magnitudes and blood flow streamlines are shown in Figure 6 for representative cases of each group before and after the endograft implantation.

Figure 4. Maximum velocities (95th percentile) for the different abdominal aorta regions before (PRE) and after (POST) implantation of the endografts. Dotted and dashed lines indicate post-endovascular aneurysm sealing (EVAS) and post-endovascular aneurysm repair (EVAR) cases, respectively. ††P < .01 post-EVAS compared to pre-EVAS. §P < .05, §§P < .01 EVAS compared to EVAR.

Figure 5. Maximum wall shear stress (95th percentile) for the different abdominal aorta regions before (PRE) and after (POST) implantation of endografts. Dotted and dashed lines indicate post-endovascular aneurysm sealing (EVAS) and post-endovascular aneurysm repair (EVAR) cases, respectively. ††P < .01 post-EVAS compared to pre-EVAS. §P < .05 EVAS compared to EVAR.

Discussion

Significant anatomic modifications are visible after EVAS compared to EVAR, with 3 main consequences for the fluid dynamics: (1) a proximal pressure modification at the level of the renal arteries, (2) an acceleration of blood velocity inside the stents that remained high at the stent outlet, and (3) higher peak WSS values observed at the iliac arteries. These flow disturbances were accurately quantified in our simulations using patient-specific models and should be analyzed separately to assess the effects of each endograft configuration on hemodynamics.

In preoperative simulations, pressure values in the proximal abdominal aorta for both groups were less than 1 mm Hg above the reference values set at the iliac outlet (Figure 3, solid lines). Pressure values increased to 2.3 mm Hg after EVAS, whereas no significant changes were observed after EVAR (Figure 3 and Table 2). This pressure modification in the proximal abdominal aorta can be probably explained by the radial mismatch introduced after EVAS, which virtually shifted upward the aortic bifurcation (Supplemental Figure 1). The enlargement of the aneurysm sac lumen compared to mean aortic size was similar between groups, as can be observed in preoperative scans (Figure 2). Nevertheless, while the aortic lumen seemed to recover a normal size after EVAR, a significant shrinkage was imposed by the EVAS system, where blood was forced to circulate into a pair of 10-mm stents (Figure 2). The suprarenal aortic geometry did not differ between groups. How this suprarenal pressure change could impact the renal flow or function is difficult to predict at this stage. Recently, Boersen et al have compared in vitro the effects of EVAR versus EVAS endografts on aortic hemodynamics using PIV, and they found that the different stent designs did not alter suprarenal flow, although WSS patterns inside the renal arteries were disturbed.[6] In our simulations, peak blood velocities around the renal arteries in both groups remained unchanged (Figure 4). We also found a high variability in peak WSS values within the suprarenal aortic region, but no significant differences were observed between groups (Figure 5). Our measurements were concentrated on the aortic wall and not in the renal arteries. Further studies will need to be undertaken to evaluate the impact of pressure change at that level.

Since patients in this study were treated in 2014, we did not employ the most recent instructions for use (IFUs) of the EVAS system. Nevertheless, the original IFUs were respected in all Nellix cases, inducing the difference observed in proximal neck length between the 2 groups (Table 1). The EVAS in short-neck aneurysm has already been reported with bad outcomes at long term,[17] but since we did not aim to evaluate outcomes in terms of aneurysm exclusion by both endografts, we believe that these differences should not have influenced the postoperative simulation.

Blood velocities inside the EVAS endoframe stents were higher compared to EVAR, with peaks around 60 versus 20 cm/s, respectively (Figure 4). More importantly, blood velocity remained high at the iliac level after EVAS. As shown in
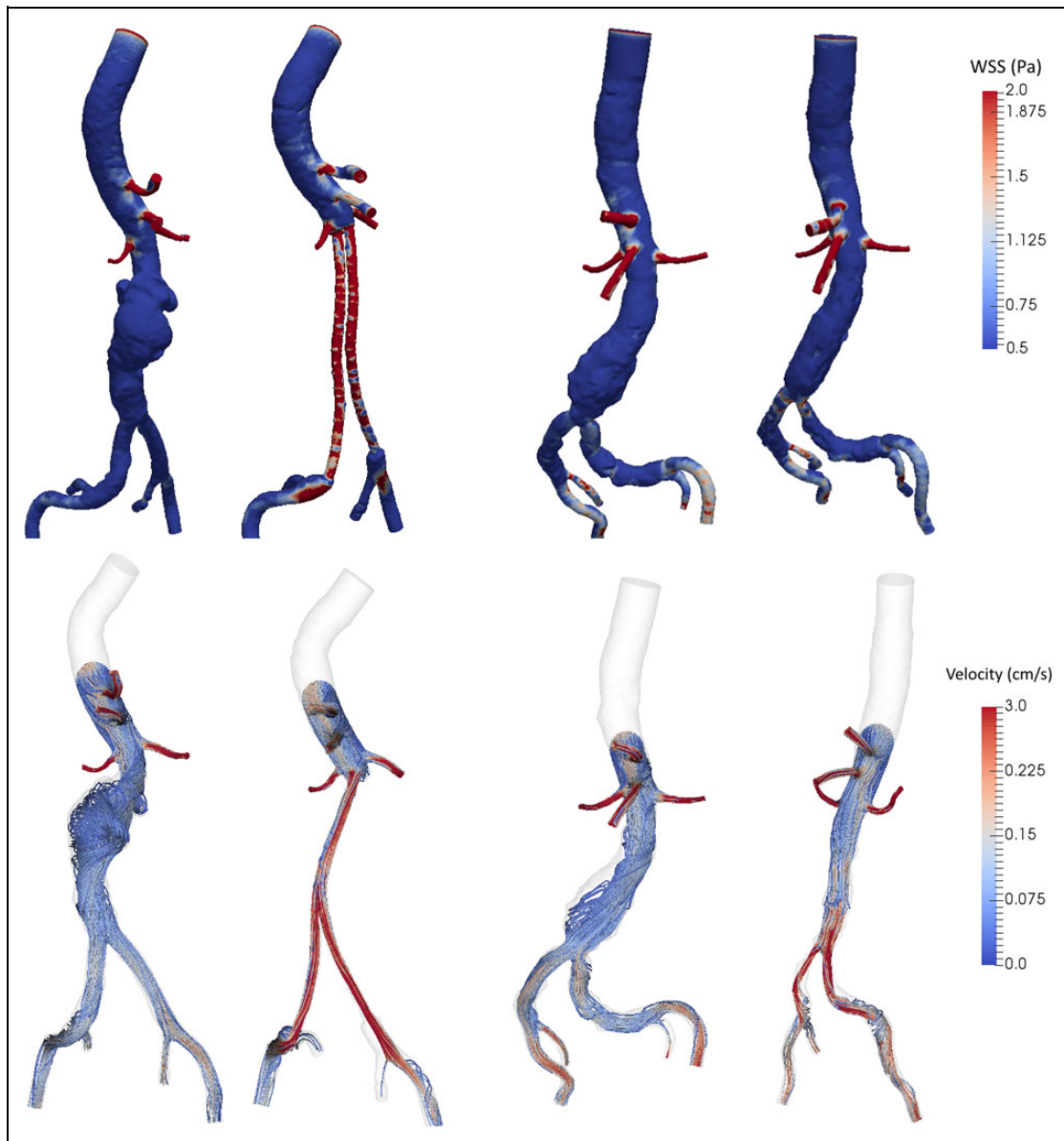
Figure 6. Qualitative wall shear stress magnitudes and blood flow streamlines before and after the implantation of the endografts. Left: A representative patient of the endovascular aneurysm sealing (EVAS) group. Right: A representative patient of the endovascular aneurysm repair (EVAR) group.

preoperative simulations, blood velocity slowed down inside the aneurysm region, probably due to the aortic lumen expansion. A distal acceleration was observed, associated with the CSA reduction (Figure 2). We believe that the dramatic post-EVAS reduction in CSA produced a significant acceleration on blood velocity, which remained high at the limbs, causing WSS values to rise. Qualitative differences between groups in WSS and streamlines are shown for representative patients in Figure 6. It is clear that after endograft implantation in both groups, the turbulent and disordered flow pattern observed inside the aneurysm sac was accelerated through the limbs when the arterial lumen recovered its normal size. However, as shown in our study, the magnitude of this acceleration depended on the particular stent configuration and was higher after EVAS.

A decrease in iliac artery angulations was observed after EVAS[5] and a reduction in iliac tortuosity was reported after EVAR.[18] The evidence of a stronger flow jet at the endograft outlet might be connected to this latter apparent straightening of the iliac arteries. Our results confirmed that the EVAR procedure provided less hemodynamic disturbances in terms of pressure, blood velocity, and WSS with respect to EVAS, probably because AFX endograft is more conformable to the blood flow due to a more physiologic configuration and the anatomical fixation system.

As recently anticipated,[19] our findings confirm that a more physiologic configuration of an endograft provides the least hemodynamic disturbance to reconstruct the aortic bifurcation. Post-EVAS studies with longer follow-up are required to

investigate the impact of pressure, flow, and WSS changes observed in our simulations on graft migration, endoleaks, and limb complications. Indeed, such mechanical stimuli are well known to impact on cell function and aortic wall remodeling.[20] Some researchers are currently investigating the Nellix migration[21] and endoleak risks.[22] Proximal rather than distal migrations of the Nellix prosthesis in the caudal direction were recently reported, although it seems not to have a clinical significance in terms of endoleaks incidence. Globally, a low total endoleak rate has been reported with the EVAS system, although some novel type of events like the long-term separation of the polymer-filled endobags should be further investigated. These specific forms of migration could be associated with the proximal pressure changes and the distal flow perturbations evidenced in our study. The EVAS system is also being analyzed in terms of aortic stiffness mismatch at this level using pulse wave velocity,[23] the polymer filling volume,[24] and the volumetric sac expansion,[3] which are particularly important to predict aneurysms rupture.[25] To our knowledge, our study is the first to conduct a CFD simulation to assess pre- and post-EVAS hemodynamic changes using patient-specific anatomies. All these efforts are articulated with recent in vitro comparisons of different endograft configurations,[19] aimed at better understanding the varying clinical results and helping the specialist to choose the proper endograft model.

Some limitations of this study should be mentioned. First, our results should be analyzed with caution due to the small number of participants. The pre- and postoperative comparisons were more robust due to the paired nature of the tests. Although pressure, velocity, and WSS values showed tendencies that reasonably explained the aortic hemodynamic changes observed in our study, simulations in larger cohorts should be scheduled. Second, standard CFD simplifying assumptions were adopted, including the Newtonian, incompressible, and stationary fluid, and conditions were adopted using literature averaged values. During previous CFD simulations in cerebral aneurysms, we concluded that resulting CFD variables like velocity and WSS for steady state simulations were equivalent to averaging the same variables over the cardiac cycle for a transient simulation.[11] Since we are assessing mostly pressure drop, velocity, and WSS at specific locations over a period of time longer than the cardiac cycle, in the current study, we performed steady state instead of transient CFD simulations, with an additional benefit of a considerable computational time reduction. The pressure reference in our study was set at the limb extremes, to assess the supplementary hydrostatic pressure required by the fluid to pass through the implanted prosthesis that reduces the lumen area. For a more precise wall pressure estimation, fluid–structure interaction models with pulsatile flows can be proposed.[26,27] Blood flow at the outlet of the renal, mesenteric, and celiac arteries was assumed constant before and after the endograft implantation. The GDM used to assess the aortic lumen mesh was conceived to expand until the external e-PTFE border and the eventual effects of the stent struts on the blood flow were neglected in our simulation. Finally, only aortic lumen was segmented, leaving thrombotic

structures outside the simulated models. Potential errors related to the lumen–thrombus interface segmentation should also be considered. Nevertheless, these systematic errors were present in patients of both groups, where aneurysms sizes were similar and no endoleaks were detected. Further studies are envisaged using magnetic resonance techniques to incorporate dynamic measurements as patient-specific blood flow magnitudes and aortic wall distensibility.

Conclusion

Based on patient-specific 3-D models employed in CFD simulations before and after endovascular treatment of AAA, we found significant modifications of fluid dynamics after EVAS with respect to EVAR. After EVAS, a 2-fold pressure increase was observed at the renal arteries level compared to EVAR and the 3-fold acceleration of blood velocity inside the EVAS stents induced a 60% increase in blood velocity at the iliac arteries level and a concomitant increase in peak WSS. These alterations might be explained by the significant modification of the abdominal aorta anatomy after EVAS compared to EVAR. Further studies including more participants should be conducted to confirm these preliminary results.

ORCID iD

Javier Dottori http://orcid.org/0000-0002-1972-8523
Damian Craiem http://orcid.org/0000-0003-1065-799X

Supplemental Material

Supplemental material for this article is available online.

References

1. Bockler D, Holden A, Thompson M, et al. Multicenter nellix endovascular aneurysm sealing system experience in aneurysm sac sealing. *J Vasc Surg*. 2015;62(2):290-298.
2. Krievins DK, Holden A, Savlovskis J, et al. Evar using the nellix sac-anchoring endoprosthesis: treatment of favourable and adverse anatomy. *Eur J Vasc Endovasc Surg*. 2011;42(1):38-46.
3. Shaikh U, Chan TY, Oshin O, et al. Changes in aortic volumes following endovascular sealing of abdominal aortic aneurysms with the nellix endoprosthesis. *J Endovasc Ther*. 2015;22(6): 881-885.
4. Casciaro ME, El-Batti S, Chironi G, et al. Deformable surface model for the evaluation of abdominal aortic aneurysms treated

with an endovascular sealing system. *Ann Biomed Eng*. 2016; 44(5):1381-1391.

5. Boersen JT, Schuurmann RC, Slump CH, et al. Changes in aortoiliac anatomy after elective treatment of infrarenal abdominal aortic aneurysms with a sac anchoring endoprosthesis. *Eur J Vasc Endovasc Surg*. 2016;51(1):56-62.

6. Boersen JT, Groot Jebbink E, Versluis M, et al. Flow and wall shear stress characterization after endovascular aneurysm repair and endovascular aneurysm sealing in an infrarenal aneurysm model. *J Vasc Surg*. 2017;66(6):1844-1853.

7. Larrabide I, Geers AJ, Morales HG, Aguilar ML, Rufenacht DA. Effect of aneurysm and ICA morphology on hemodynamics before and after flow diverter treatment. *J Neurointerv Surg*. 2015;7(4):272-280.

8. Larrabide I, Villa-Uriol MC, Cardenes R, et al. Angiolab—a software tool for morphological analysis and endovascular treatment planning of intracranial aneurysms. *Comput Methods Programs Biomed*. 2012;108(2):806-819.

9. Diethrich EB. Novel sealing concept in the endologix afx unibody stent-graft. *J Cardiovasc Surg (Torino)*. 2014;55(1):93-102.

10. Weller HG, Tabor G, Jasak H, Fureby C. A tensorial approach to computational continuum mechanics using object-oriented techniques. *Comput Phys*. 1998;12:620-631.

11. Geers AJ, Larrabide I, Morales HG, Frangi AF. Approximating hemodynamics of cerebral aneurysms with steady flow simulations. *J Biomech*. 2014;47(1):178-185.

12. Morales HG, Larrabide I, Geers AJ, Aguilar ML, Frangi AF. Newtonian and non-newtonian blood flow in coiled cerebral aneurysms. *J Biomech*. 2013;46(13):2158-2164.

13. Bernardini A, Larrabide I, Morales HG, et al. Influence of different computational approaches for stent deployment on cerebral aneurysm haemodynamics. *Interface focus*. 2011;1(3):338-348.

14. Osada T. Physiological aspects of the determination of comprehensive arterial inflows in the lower abdomen assessed by doppler ultrasound. *Cardiovasc Ultrasound*. 2012;10:13.

15. Osada T, Katsumura T, Hamaoka T, et al. Reduced blood flow in abdominal viscera measured by doppler ultrasound during one-legged knee extension. *J Appl Physiol (1985)*. 1999;86(2):709-719.

16. Osada T, Murase N, Kime R, et al. Arterial blood flow of all abdominal-pelvic organs using doppler ultrasound: range, variability and physiological impact. *Physiol Meas*. 2007;28(10): 1303-1316.

17. Psacharopulo D, Ferri M, Ferrero E, et al. Comparison of outcomes for short-neck and juxtarenal aortic aneurysms treated with the nellix endograft versus conventional endovascular aneurysm sealing. *J Vasc Surg*. 2017;66(5):1371-1378.

18. Coulston J, Baigent A, Selvachandran H, Jones S, Torella F, Fisher R. The impact of endovascular aneurysm repair on aortoiliac tortuosity and its use as a predictor of iliac limb complications. *J Vasc Surg*. 2014;60(3):585-589.

19. Groot Jebbink E, Mathai V, Boersen JT, et al. Hemodynamic comparison of stent configurations used for aortoiliac occlusive disease. *J Vasc Surg*. 2017;66(1):251-260 e251.

20. Back M, Gasser TC, Michel JB, Caligiuri G. Biomechanical factors in the biology of aortic wall and aortic valve diseases. *Cardiovasc Res*. 2013;99(2):232-241.

21. England A, Torella F, Fisher RK, McWilliams RG. Migration of the nellix endoprosthesis. *J Vasc Surg*. 2016;64(2):306-312.

22. Swaelens C, Poole RJ, Torella F, McWilliams RG, England A, Fisher RK. Type IIIb endoleak and relining: a mathematical model of distraction forces. *J Endovasc Ther*. 2016;23(2): 297-301.

23. Casciaro M, Alfonso M, Craiem D, Alsac J, El-Batti S, Armentano R. Predicting the effect on pulse wave reflection of different endovascular repair techniques in abdominal aortic aneurysm using 1D patient-specific models. *Health and Technology*. 2016;6(3):173-179.

24. Boersen JT, van den Ham LH, Heyligers JM, et al. Validation of pre-procedural aortic aneurysm volume calculations to estimate procedural fill volume of endobags in endovascular aortic sealing. *J Cardiovasc Surg (Torino)*. 2017;58(5):674-679.

25. Cheng LF, Cheung KF, Chan KM, et al. Early enlargement of aneurysmal sac and separation of endobags of nellix endovascular aneurysm sealing system as signs of increased risk of later aneurysm rupture. *Cardiovasc Intervent Radiol*. 2016;39(11): 1654-1657.

26. Frauenfelder T, Lotfey M, Boehm T, Wildermuth S. Computational fluid dynamics: hemodynamic changes in abdominal aortic aneurysm after stent-graft implantation. *Cardiovasc Intervent Radiol*. 2006;29(4):613-623.

27. Li Z, Kleinstreuer C. Fluid–structure interaction effects on sac-blood pressure and wall stress in a stented aneurysm. *J Biomech Eng*. 2005;127(4):662-671.